Universiteit Utrecht

Master scriptie

Optical transmission through a subwavelength gold square nanohole array

Author:
Floor Kamphorst
3020983

Supervisor:
Dr. Dries van Oosten

July 2, 2012

Abstract

In 1998 Ebbesen and co-workers discovered the extraordinary optical transmission through a subwavelength silver nano hole array. Here we measure the transmittance of a subwavelength gold square nano hole array. We study the transmittance as a function of hole size and as a function of array size.

Comparing the results of the 2500 μm^2 array with the 930 μm^2 array, we conclude the array size is an important factor for the transmittance profile. Transmittance of the 2500 μm^2 array follows a clear Fano-profile and has a larger transmittance.

For the transmittance dependent on hole size, we can make a distinction between holes that do not support transverse electromagnetic waves, *i.e.* that are in cutoff, and holes that are not in cutoff. The normalized transmission for arrays that are not in cutoff is not dependent on hole size. This result shines a new light on the extra ordinary transmission.

Contents

Chapter 1

Introduction

1.1 Scientific background

In 1998 Ebbesen and co-workers measured the transmission of light through a subwavelength silver nano hole array [5]. When they normalized the transmission to the open area, the transmittance profile was not constant. Some wavelengths had reduced transmittance, whereas others were enhanced.

At the time, the observations were not explained theoretically. Until then, it was thought that the transmittance depended on wavelength as (d/λ^4), with d the radius of the apperture [2]. Because the transmission was not explained theoretically, Ebbesen named it extraordinary optical transmission.

Since its discovery, the factors that could influence the extraordinary transmission are extensively researched. The type of material only plays a role on the surface layer, with a thickness of the skin depth [8]. Van der Molen *et. al.* found that the transmission appears to be stronger and more pronounced in good conductors [19].

According to Ebbesen [5] the enhanced wavelength (or the position of the transmittance maximum) shifts with respect to the angle of the incident light. The transmittance has maxima for certain wavelengths. The position of these maxima depend on hole shape [19, 10] and the grating period [5, 18].

The transmittance is influenced by the polarization of the incident light [6] and the properties of the holes. Also hole depth and size influence the transmittance. The bigger the holes, the larger the transmittance [5], but the transmittance decreases linearly with increasing hole depth [4].

1.2 Different theoretical explanations

Various authors tried to model the extraordinary optical transmission. In these explanations, guided surface modes, especially surface plasmon polaritons (SPPs), are mentioned as a contributing factor [5, 16, 9, 1, 12, 14].

There are also authors that use other models to describe the extraordinary transmission [3, 13, 11]. Although these explanations state that SPPs have nothing to do with the extraordinary transmission, or have even a negative contribution [3, 13], they all use certain aspects of the models that do include SPPs.

Instead of surface plasmons, the extraordinary transmission is explained by surface currents [3] or *composite diffracted evanescent waves* (CDEWs) [13]. The CDEW-theory by Lezec and Thio explaines the extraordinary transmission as a superposition of diffraction modes. Although these theories do not use guided modes, they do describe a wave that is bound to the surface of the array.

Lalanne *et. al.* [11] give a numerical description for the transmittance in the far and near field. They use a SPP mode, which mainly contributes to the far field. In the near field there is another contribution to the transmittance at the surface. This contribution is given by a creeping wave, which has a high transmittance close to the surface, but is not bound to that surface. The contribution of the creeping wave is significant for short distances ($\lambda d < 1$).

Although this introduction focuses on models that do not include SPPs, current consensus states that the array couples light into a guided mode. The transmission is enhanced by the guided mode, which leads eventually to the transmittance pattern found by Ebbesen [5]. The contribution of SPPs will in greater length be discussed in Chapter 2.

1.3 Experimental context

The near field of the transmission of a metal nano hole array has local intensity maxima. Atoms can be manipulated with a strong electromagnetic field. We want to study the interaction between cold Rubidium atoms and the near field of a nano hole array. How does the size of our sample influence the transmission? What is the influence of the hole size?

The transmission through a subwavelength hole in a real metal film is larger than predicted by Bethe and Bouwkamp [2]. But when the transmission through an array is normalized to the transmission through a single hole, the enhancement (per hole) of the array is up to a factor of 7 [13].

The extraordinary transmission is mainly ascribed to a SPP contribution.

The larger the array, the stronger the coupling between the array and the SPP can be. We therefore think the transmission spectrum is largely influenced by the finite size of the array. We will study the transmission for different array sizes. This way we want to get a better view on the role that the array size plays in the extraordinary transmission.

Chapter 2

Theory

2.1 Introduction

We study the transmittance of white light through a gold nano hole array. When white light is incident on a thin metal grating, part of the light will be reflected, part will be transmitted and part of the light will be diffracted. Because we have a grating structure, diffraction is described by the grating equation (or Bragg-condition)

$$m\lambda = d(\sin\theta_i + \sin\theta_d). \tag{2.1}$$

In this equation, m is an integer, d is the grating period, θ_i is the angle of incidence and θ_d is the angle of diffraction. With a given angle of incidence, for a certain wavelength $\lambda_{\text{Rayleigh}}$, the angle of diffraction will be 90°. The wave will propagate along the surface of the grating. For wavelengths bigger than this wavelength, there is no diffraction. In other words: a diffraction channel is shut off, and for those wavelengths, the far field intensity is smaller. This abrupt change in the intensity is called Rayleigh's anomaly. In our results this anomaly appears as a kink in the transmittance.

One of the waves that is outcoupled at Rayleigh's anomaly, can have a corresponding SPP with a wavelength that matches the grating period. For metal gratings this wave is then coupled to a guided surface mode. The coupled wave has only two dimensions and a fixed angle of either incidence or diffraction. This leads to a diminished intensity for this one wavelength. This is known as Wood's anomaly, and the resulting guided surface modes are called surface plasmon polaritons (SPPs).

When measuring the laser power, we recognize a Fano-profile. This means there is a direct contribution that interferes with a spectrally narrow indirect contribution. In our case, the direct transmission and the enhanced

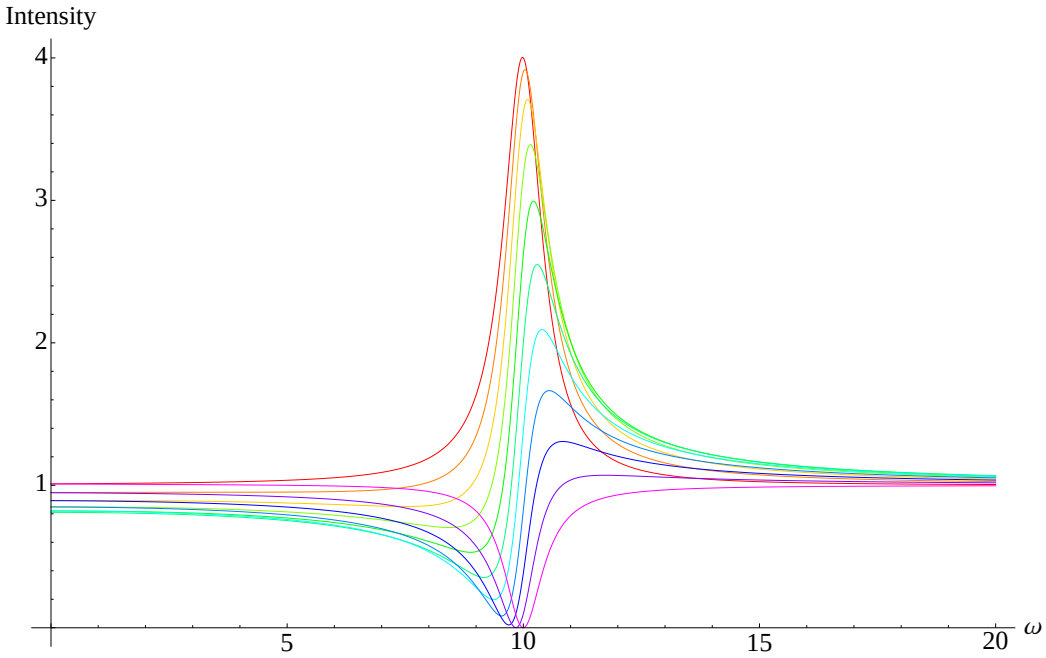

Figure 2.1: Intensity of the interference of a Lorentz-oscilator and a background field as function of the frequency. The Intensity is plotted for several phases of the field, -0.5 π (red) and 0.5 π (pink).

transmission through the holes. Mathematically we can describe this by a background with a phase (the direct transmission) that interferes with a Lorentz-oscillator. Verhagen [21] showed that this model gives an accurate description of the power measurements. In Figure 2.1 the Fano-profile is illustrated for different phases of the plane wave.

2.2 Waveguide theory

The holes in our sample can be described with classical waveguide theory. The boundary conditions for the inner wall of a waveguide are [7]

$$E_{||} \stackrel{\rightarrow}{=} 0 \tag{2.2}$$

$$B_{\perp} = 0. \tag{2.3}$$

Figure 2.2 depicts a rectangular waveguide with sides of length a and b.

In this waveguide transverse electric waves can propagate. Due to the boundary conditions, the magnetic field only has a z-component. When we solve the magnetic field for the boundary conditions we get the following

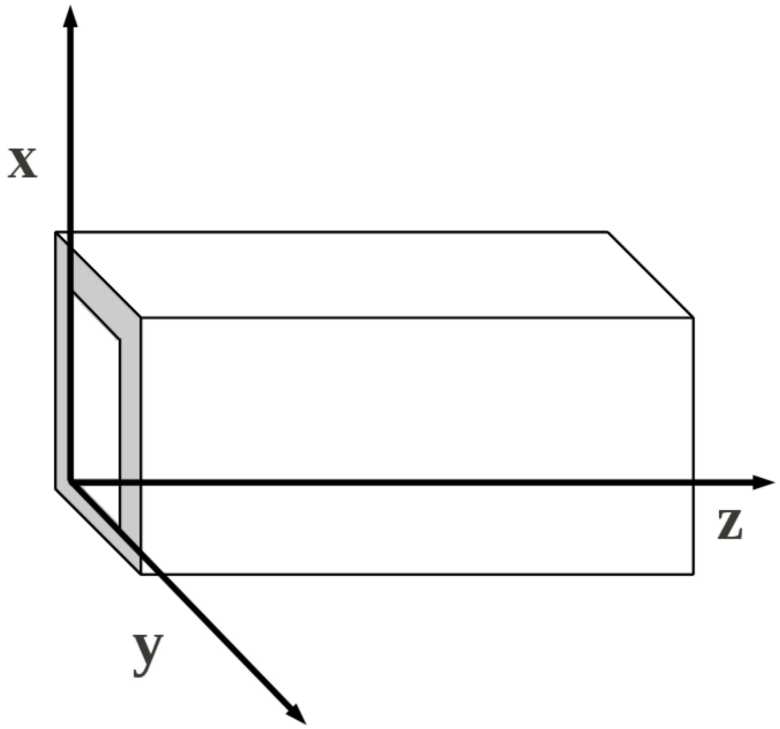

Figure 2.2: Square waveguide with dimensions a and b.

wavenumber

$$k = \sqrt{(\omega/c)^2 - \pi^2[(m/a)^2 + (n/b)^2]}. \tag{2.4}$$

When the wavelength is smaller than b/2 ($a \geq b$), the wavenumber is imaginary and the wavelength is not supported by the waveguide. The electromagnetic wave evanescently penetrates the hole, and there is almost no transmission for these wavelengths.

2.3 Surface Plasmon Polaritons

Qualitatively, surface plasmons can be understood as oscillating modes of the electron cloud in the metal on a metal-dielectric interface. These modes can be excited by electromagnetic waves (light). The excited modes result in a traveling wave that is bound to the interface. We call these surface waves surface plasmon polaritons (SPPs), and they follow naturally from solving Maxwell's equations [7] for the appropriate boundary conditions.

We now consider the interface between a metal and a dielectric medium. The boundary conditions for an electromagnetic wave that can exist on the

interface between those two media are given by

$$\vec{n} \times \vec{E_1} = \vec{n} \times \vec{E_2} \tag{2.5}$$

$$\vec{n} \times \vec{H_1} = \vec{n} \times \vec{H_2} \tag{2.6}$$

$$\vec{n} \cdot \vec{D_1} = \vec{n} \cdot \vec{D_2} \tag{2.7}$$

$$\vec{n} \cdot \vec{B_1} = \vec{n} \cdot \vec{B_2}. \tag{2.8}$$

The first two conditions 2.5, 2.6 make sure that the fundamental magnetic and electric fields are equal when we look from both sides to the interface. The third and forth boundary condition 2.7 , 2.8 state that when the metal is polarized, the charge is the same for both sides of the interface.

We can rewrite this boundary conditions in the following form

$$E_{\parallel,1} = E_{\parallel,2} = E_{\parallel} \tag{2.9}$$

and

$$H_{\parallel,1} = H_{\parallel,2} = H_{\parallel}. \tag{2.10}$$

The perpendicular components of the electric field are not equal. So $E_{\perp,1} \neq E_{\perp,2}$, but the perpendicular components of the displacement fields are

$$D_{\perp,1} = D_{\perp,2} = D_{\perp} \tag{2.11}$$

and

$$B_{\perp,1} = B_{\perp,2} = B_{\perp}. \tag{2.12}$$

When we assume that both media are non magnetic, so $\mu_1 = \mu_2 = 1$, also the perpendicular components of the H-field are equal

$$H_{\perp,1} = H_{\perp,2} = H_{\perp}. \tag{2.13}$$

Now let's try the following solution for the electromagnetic wave

$$\vec{H_j} = (0, \tilde{H}, 0)\mathrm{e}^{\mathrm{i}(\mathrm{k_x}\hat{\mathrm{x}} + \mathrm{k_{z_j}}\hat{\mathrm{z}} - \omega \mathrm{t})} \tag{2.14}$$

$$\vec{E_j} = (\tilde{E}_x, 0, \tilde{E}_{z_j})\mathrm{e}^{\mathrm{i}(\mathrm{k_x}\hat{\mathrm{x}} + \mathrm{k_{z_j}}\hat{\mathrm{z}} - \omega \mathrm{t})}. \tag{2.15}$$

When we put these equations into the wave equation

$$\nabla^2 \vec{H} = \frac{\epsilon}{c^2} \frac{\partial^2}{\partial t^2} \vec{H}, \tag{2.16}$$

we get

$$\frac{\partial^2}{\partial t^2} \vec{H} = \frac{\partial}{\partial t} - i\omega(0, \tilde{H}, 0)\mathrm{e}^{\mathrm{i}(\mathrm{k_x}\hat{\mathrm{x}} + \mathrm{k_{z_j}}\hat{\mathrm{z}} - \omega \mathrm{t})},$$

$$= -\omega^2(0, \tilde{H}, 0)\mathrm{e}^{\mathrm{i}(\mathrm{k_x}\hat{\mathrm{x}}+\mathrm{k_{z_j}}\hat{\mathrm{z}}-\omega\mathrm{t})} \tag{2.17}$$

and

$$\nabla^2\vec{H} = (\frac{\partial^2}{\partial x^2} + \frac{\partial^2}{\partial y^2} + \frac{\partial^2}{\partial z^2})(0, \tilde{H}, 0)\mathrm{e}^{\mathrm{i}(\mathrm{k_x}\hat{\mathrm{x}}+\mathrm{k_{z_j}}\hat{\mathrm{z}}-\omega\mathrm{t})},$$
$$= (-k_x^2 - k_{z_j}^2)(0, \tilde{H}, 0)\mathrm{e}^{\mathrm{i}(\mathrm{k_x}\hat{\mathrm{x}}+\mathrm{k_{z_j}}\hat{\mathrm{z}}-\omega\mathrm{t})}. \tag{2.18}$$

From the wave equation 2.16 we now know

$$k_x^2 + k_{z_j}^2 = \frac{\epsilon\omega^2}{c^2}, \tag{2.19}$$

which leads to the following dispersion relation

$$k_j^2 = k_x^2 + k_{z_j}^2 = \epsilon_j k_0^2, \tag{2.20}$$

with $k_0 = \omega/c$.

From the Maxwell equations we know that $\nabla \cdot \vec{D} = \rho_f$. As there are no free charges in our system, we get

$$\nabla \cdot \vec{D} = (\frac{\partial}{\partial x} + \frac{\partial}{\partial y} + \frac{\partial}{\partial z})(\tilde{D}_x, 0, \tilde{D}_{z_j})\mathrm{e}^{\mathrm{i}(\vec{\mathrm{k}}\cdot\vec{\mathrm{x}}-\omega\mathrm{t})}$$
$$= (\mathrm{ik_x D_x} + \mathrm{ik_{z_j} D_{z_j}})$$
$$= 0 \tag{2.21}$$

Assuming we are dealing with linear media, we know [7]

$$D_x = \epsilon_j E_x,$$

and

$$D_{z_j} = \epsilon_j E_{z_j}. \tag{2.22}$$

When we insert this in 2.21, we get

$$\mathrm{i}\epsilon(\mathrm{k_x E_x} + \mathrm{k_{z_j} E_{z_j}})\mathrm{e}^{\mathrm{i}(\vec{\mathrm{k}}\cdot\vec{\mathrm{x}}-\omega\mathrm{t})} = 0, \tag{2.23}$$

so

$$k_x E_x + k_{z_j} E_{z_j} = 0. \tag{2.24}$$

Notice equation 2.24 only holds within one medium, and does not apply on the surface. Recalling boundary condition 2.11 in combination with 2.22, we know that

$$\epsilon_1 \tilde{E}_{z_1} = \epsilon_2 \tilde{E}_{z_2}. \tag{2.25}$$

With the combination of the following equations 2.20, 2.24 ,2.25, we can find the dispersion relation for the wave vector in the two media. First we

eliminate k_x^2 from equation 2.20, because it has the same value at the interface for both media. This gives us

$$\epsilon_1 k_0^2 - k_{z_1}^2 = \epsilon_2 k_0^2 - k_{z_2}^2. \tag{2.26}$$

From the divergence of the displacement fields 2.21 we can isolate the x-component of the electric field

$$k_{z_j} E_{z_j} + k_x E_x = 0. \tag{2.27}$$

For the separate media, this means

$$k_{z_1} \tilde{E}_{z_1} = -k_x \tilde{E}_x, \tag{2.28}$$

and

$$k_{z_2} \tilde{E}_{z_2} = -k_x \tilde{E}_x, \tag{2.29}$$

giving us the relation for the z-components of the electric field:

$$k_{z_1} \tilde{E}_{z_1} = k_{z_2} \tilde{E}_{z_2}. \tag{2.30}$$

By using boundary condition 2.25, the divergence of the displacement field 2.21 and eliminating E_{z_1}, we get

$$k_{z_1} = k_{z_2} \frac{\epsilon_1}{\epsilon_2}, \tag{2.31}$$

or

$$k_{z_2} = \frac{\epsilon_2}{\epsilon_1} k_{z_1}. \tag{2.32}$$

Using 2.32, we can eliminate k_{z_2} from 2.20, giving us

$$k_{z_1}^2 = \frac{\epsilon_1^2}{\epsilon_2 + \epsilon_1} k_0^2. \tag{2.33}$$

Using the same method we can also find

$$k_{z_2}^2 = \frac{\epsilon_2^2}{\epsilon_2 + \epsilon_1} k_0^2. \tag{2.34}$$

This result 2.33 we can put into the dispersion relation 2.20

$$k_x^2 = k_0^2 [\frac{\epsilon_1 \epsilon_2}{\epsilon_2 + \epsilon_1}]. \tag{2.35}$$

We now can insert values for the electric constant into the dispersion relation 2.35. We choose $\epsilon_1 > 1$ for a dielectric and $\epsilon_2 < 0$ for a metal. When $\epsilon_2 < -\epsilon_1$, $k_{z_j} < 0$ (see equation 2.33), so k_{z_j} is imaginary, k_x is real and $k_x > k_0$. With these conditions we have an electromagnetic wave that propagates in the x-direction (parallel to the interface) and is evanescent in the z-direction (perpendicular to the interface). This wave we call the surface plasmon. The dispersion relation for a SPP on an air-gold interface as a function of wavelength is shown in Figure 2.3.

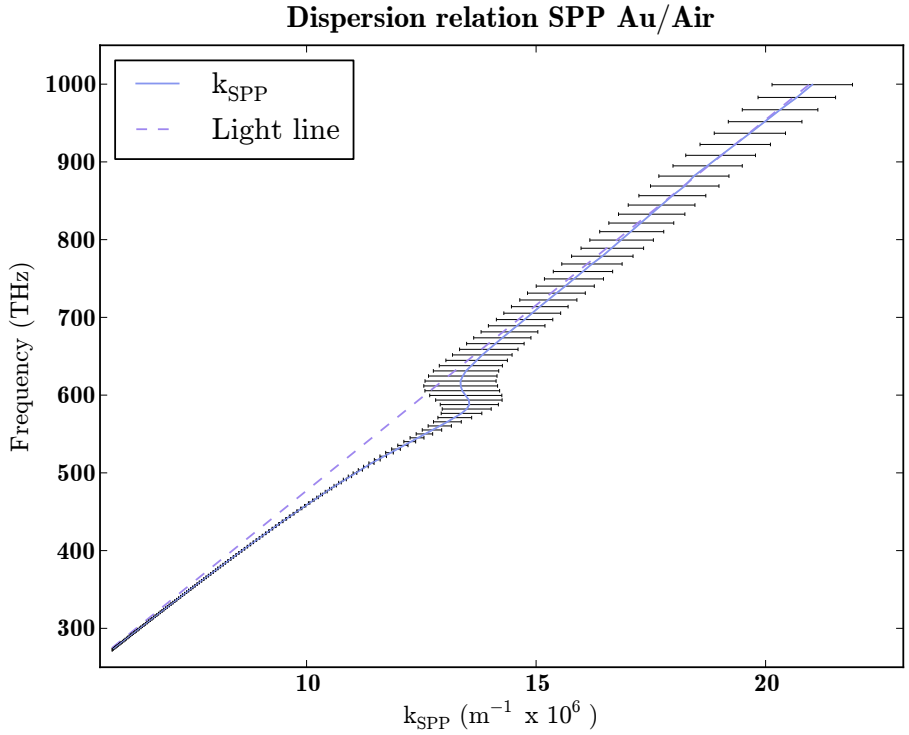

Figure 2.3: This graph gives the relation between the frequency in vacuum and the real part of the wavenumber of the SPP. The horizontal bars show the imaginary part of the wavenumber, Im$\{k_{SPP}\}$.

2.4 Coupling of light into SPPs

We have seen that electromagnetic waves can exist on the interface between a metal and a dielectric (see section 2.3). But how does light couple into a SPP? We will first look at the behavior of an electromagnetic plane wave when it meets a disturbance in space in the x-plane, with a certain coupling t(x). A schematic overview is given in Figure 2.4.

The field of the incoming wave is given by

$$E_{\text{in}} = E_0 \mathrm{e}^{\mathrm{ik}_{\parallel}\mathrm{x}} \mathrm{e}^{\mathrm{ik}_{\perp}\mathrm{z}}. \tag{2.36}$$

When we define the coupling as follows

$$t(x) = t_0, \tag{2.37}$$

the transmitted wave will be given by

$$E_{\text{out}} = t(x) E_{\text{in}}, \tag{2.38}$$

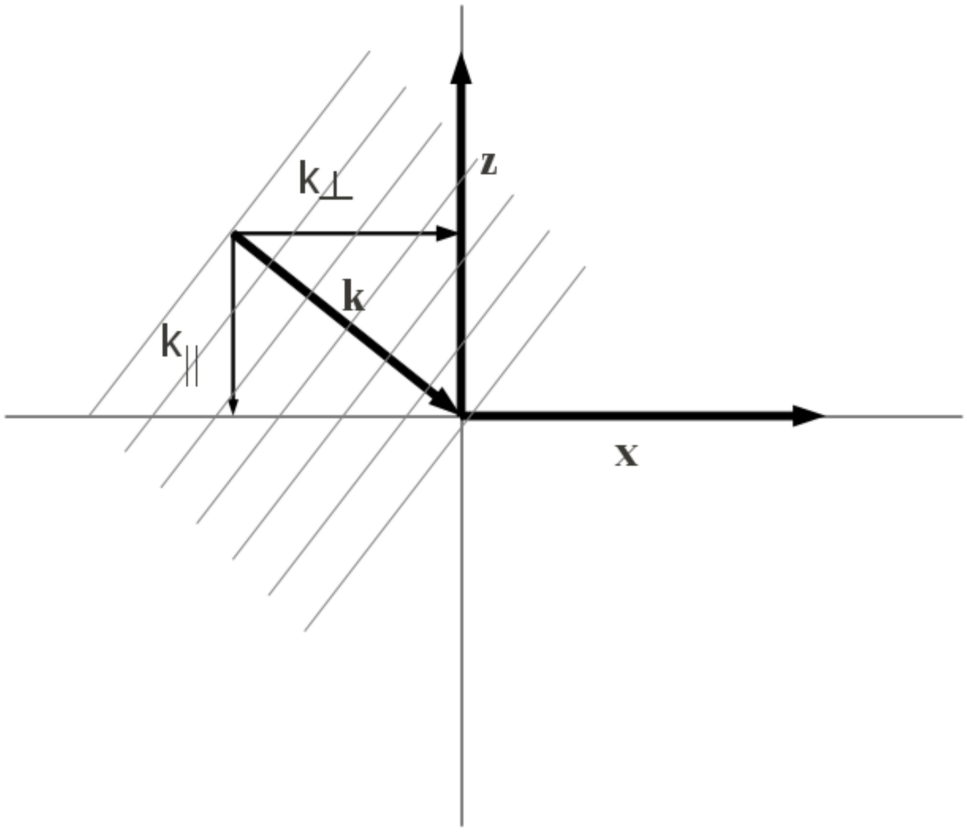

Figure 2.4: A plane wave is incident on a material with transmittivity t(x). In the overview the x, z, and k-vectors are given.

$$E_{\text{out}} = t_0 E_0 \mathrm{e}^{\mathrm{i}k_{\parallel}x} \mathrm{e}^{\mathrm{i}k_{\perp}z}. \tag{2.39}$$

The wavenumber of the incoming wave is given by $k_0 = \sqrt{k_{\parallel}^2 + k_{\perp}^2}$. Because of energy conservation, the outcoming wave has the same wavenumber k_0. We will now look what will happen when the outcoming wave couples to a SPP mode on the interface. The parallel component of the wavenumber needs to match the wavenumber of the SPP, $k_{\parallel} = k_{\text{SPP}}$. When we look at the dispersion relation 2.35 we know that

$$k_{\text{SPP}} = k_0 \sqrt{\frac{\epsilon_1 \epsilon_2}{\epsilon_1 + \epsilon_2}}. \tag{2.40}$$

We can see that $k_{\text{SPP}} > k_0$, which leads to an imaginary value of the perpen-

dicular component of the outcoming wavevector

$$k_\perp = \sqrt{k_0^2(1 - \frac{\epsilon_1\epsilon_2}{\epsilon_1 + \epsilon_2})}. \tag{2.41}$$

The incoming wave and the SPP mode have different values for $k_\parallel$. This means the waves will couple destructively and there will be no enhanced transmittance.

When we define the coupling with a spatial component

$$t(x) = \frac{t_0}{2i}(\mathrm{e}^{\mathrm{ik_d x}} - \mathrm{e}^{-\mathrm{ik_d x}}), \tag{2.42}$$

the outcoming wave will be given by

$$E_{\mathrm{out}} = \frac{t_0 E_0}{2i}(\mathrm{e}^{\mathrm{ik_d x}} - \mathrm{e}^{-\mathrm{ik_d x}})\mathrm{e}^{\mathrm{ik_\parallel x}}\mathrm{e}^{\mathrm{ik_\perp z}}. \tag{2.43}$$

The wavenumber of the outcoming wave will now be given by

$$\begin{aligned} k_0 &= \sqrt{(k_\parallel + k_d)^2 + k_\perp^2 - (k_\parallel - k_d)^2 - k_\perp^2} \\ &= \sqrt{4k_\parallel k_d}. \end{aligned} \tag{2.44}$$

The resulting wave has only an x-component. Here we see that a regular disturbance like a grating, can add momentum to a wave. Which leads to coupling to SPPs.

2.4.1 Extraordinary transmission

We know that there are bound modes on a dielectric metal interface, and that light can couple into these modes. But how does this help us understand the extraordinary transmission? How does the light get to the other end of the sample?

From the waveguide theory we know that holes that are in cutoff have only a small transmission. This is caused by the damping of the electric field in the waveguide and because there is only a small coupling between the incoming light and the holes.

We can increase the transmission by two means. The damping can be influenced by the hole size. The bigger the hole, the smaller the damping. The coupling to the holes can be increased when light is coupled to a guided mode on the Au/Air interface. The light will interact with more holes, and have a stronger coupling.

The increase in transmission holds only for one wavelength (Wood's anomaly). This wavelength will interfere with the direct transmission (all wavelengths), resulting in a Fano-profile of the measured laser power.

2.4.2 Collective effect

From the previous section we can learn that the larger the array is, the more light is transmitted with respect to the surface area, and the bigger the enhancement is. This means that the extraordinary transmission is an effect of the array and not an effect of the individual holes. This leads us to wonder how big our array needs to be to obtain a good Fano-profile.

Chapter 3

Method and Setup

3.1 Introduction

To measure the influence of the hole size and the size of the nano hole array on the extra ordinary transmission, we need to vary these two properties. Arrays with different hole sizes were produced. The array size was not varied, instead we varied the size of the illumination spot size on the array. The sample was attached to an xy-adjustable mount, we could bring different arrays in focus, thus varying the hole size.

3.2 Setup

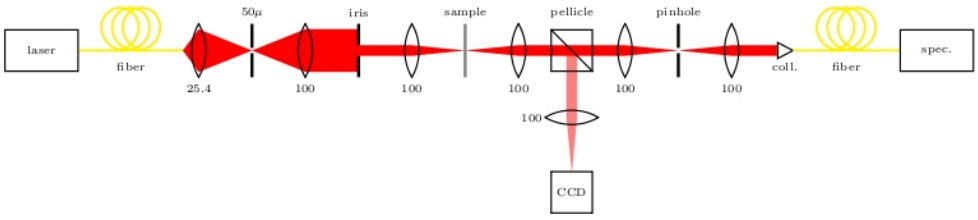

Figure 3.1: Schematic overview of the experimental setup.

We used a fiber coupled (Thorlabs 973-579-7227 FTO 30-BLUE) white ligth laser (NKT Photonics, SuperK Extreme) with an AOTF (acousto optical tunable filter) frequency sampler (NKT Photonics, SpectraK Dual). The ligth is focused on the sample, magnified by a factor $\frac{3}{10}$ and led through a beam splitter (BP108⌀1" Pellicle Beamsplitter, uncoated for 8:92 (R:T)

Split Ratio for 400-2400 nm). The main beam is focused on a pinhole and the ligth is coupled into a fiber (Ocean Optics QP200-2-VIS-BX). Eventually the power of the light is measured using a spectrometer (Ocean Optics HR2000CG-UV-NIR). The other part of the light is focused on a beam profiler (WincamD UCD12) and gives us an image of the sample. A schematic overview of the setup is given in Figure 3.1.

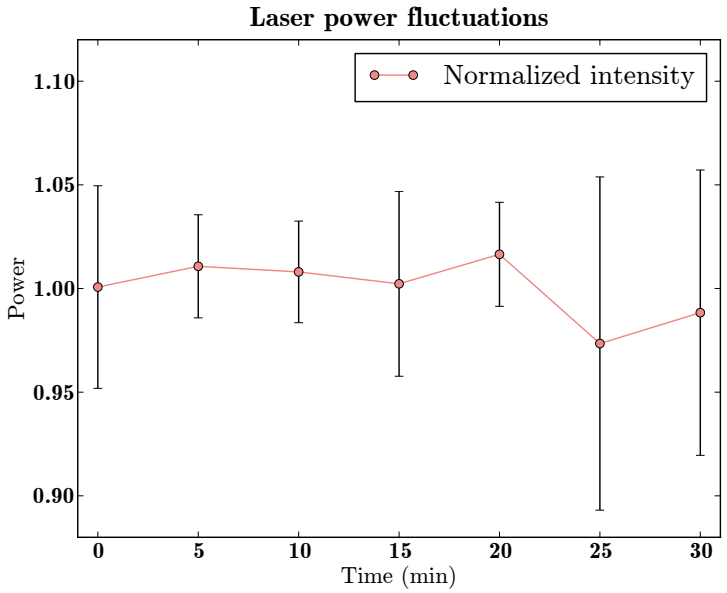

Figure 3.2: This figure shows the mean normalized laser power as a function of time. The normalization factor is given by the average power of the laser over the wavelength (700 - 900 nm) for each time interval. The errorbars show the standard deviation over λ.

The power of the laser exhibits noise and long term drift. To determine how big the drift is, we measured the power as a function of time for different wavelengths. The results are shown in Figure 3.2. The standard deviation in the power fluctuations of the laser over half an hour is between 1.3% ($\lambda = 820$ nm) and 12% ($\lambda = 850$ nm). Taking the standard deviation of the mean values for the power fluctuations (0,0136) and the mean of the standard deviations (0,0453) teaches us that the random noise in the laser is bigger than the power fluctuations. We can therefore conclude that the drift does not give us a significant error in the measurements.

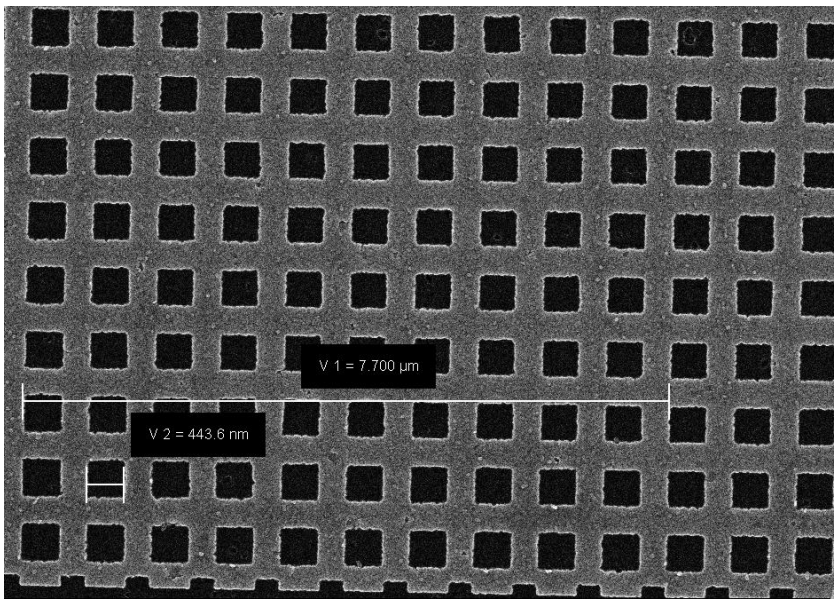

Figure 3.3: SEM-picture of the nano square hole gold array. The scale bars indicate 7.700 μm (ten times the grating period) and 443.6 nm (the hole size).

3.2.1 Sample

We produced our sample using electron beam lithography and lift-off. Each array is 50 $\times$ 50 μm. The gold is deposited using physical vapor disposition (PVD). The hole size ranges from 150 nm - 600 nm. Measurements were performed on arrays with hole size 250 nm, 300 nm, 400 nm, and 450 nm. In Figure 3.3, a typical scanning electron micrograph of an array is shown.

The choices for our sample properties lie in the context in which this research was performed. The aim is to investigate the interaction of cold Rubidium atoms with the near field of a nano hole array, because the near field of nano structures is very concentrated and can possibly be used to trap cold atoms.

We chose Au as a material for our array because it is a good conductor and does not oxidize. The better the conductor, the easier SPP modes are excited. We chose Au over Ag, which is a better conductor, because it does not oxidize, increasing the lifetime of our sample significantly. In the final setup, where measurements will be performed in vacuum, Ag is a viable option.

The grating period was aimed at 763 nm. This is the SPP-wavelength on the Au/Air interface which corresponds with a wavelength of 780 nm. For this wavelength, Rubidium atoms have the strongest transition (5s-5p). The possible interaction between the near field and the atoms is therefore

expected to be the strongest here. The SPP-wavelength as a function of wavelength of free light is plotted in Figure 2.3.

We took scanning electron microscope (SEM) pictures of our arrays. The hole sizes and grating periods of each array were measured with the scale bars of the scanning electron microscope. We measured that the actual grating period was bigger than the period we aimed for. This is due to stretching of the resist in the post baking process. The stretching is proportional to hole-size and is a linear effect. This means we can compensate for the stretching in a next sample. The actual aimed values are given in Table 3.1.

aimed hole size	average hole size (nm)	average grating period (nm)	# data points
200	211.3 ± 0	767.9 ± 0	1
250	253.5 ± 0	773.2 ± 0	1
300	311.6 ± 5.3	769.0 ± 5.3	2
350	338.0 ± 0	769.0 ± 0	2
400	401.4 ± 12.9	769.2 ± 0.9	4
450	438.4 ± 8.1	770.2 ± 0.9	6
500	495.2 ± 8.2	771.2 ± 3	8
550	545.7 ± 21.7	771.3 ± 7	12
600	591.7 ± 21.2	771.4 ± 1.5	12

Table 3.1: The average hole size and grating period for different aimed hole sizes. The aimed grating period was for all arrays the same and is 763 nm. Measurements were performed at the 250, 300, 400 and 450 nm hole arrays. Other array-sizes did not provide the quality to take good measurements.

3.3 Method

The power of the transmitted light is measured in the range of 700 nm - 900 nm, with intervals of 2 nm. For each wavelength, a reference measurement is made by measuring the power of the light on the glass. For both measurements, a dark measurement was made. Since the values of the dark measurements don't vary much with respect to wavelength (standard deviation of $\pm 0.053\%$ for the sample measurement and $\pm 0.040\%$ for the reference measurement), we measured only these two dark intensities.

The measurements were done with two different focus sizes, to illuminate a different area of the sample. This way we can test the dependence of array-size on the extraordinary transmission. The spot sizes of the focus of the beam were 18.30 ± 1.59 μm and 34.35 ± 2.10 μm in diameter.

3.3.1 Data analysis

The transmission is normalized to a reference measurement on the glass of the sample. The transmission is defined as follows

$$T = \frac{I_{\text{sample}} - I_{\text{dark,sample}}}{I_{\text{reference}} - I_{\text{dark,reference}}}, \tag{3.1}$$

with T, the transmission and I the different intensities. This normalized transmittance is plotted as a function of wavelength, and fitted to a Fano-profile.

The fit-fuction consists of two contributions: that of the single hole and of the collective effect of the array. The contribution of the single hole is given by a Bethe, Bouwkamp-like term (d/λ^4). The array contribution is given by an interference term that will give the Fano-profile to our fit.

The function is fitted to the optical frequency as a function of wavelength ($\mathrm{f}(\lambda)$), the resonance frequencies ($\mathrm{f_{r,i}}$), the damping of the resonances ($\mathrm{g_{r,i}}$) and the relative phases of the resonances to the direct transmission ($\mathrm{q_{r,i}}$). The fit function is given by

$$\mathrm{F(a, \lambda, f_{r,i}, g_{r,i}, q_{r,i}) = \frac{a}{\lambda^4} \frac{[1 + \Sigma_i q_{r,i}/e_{r,i}(\lambda)]^2}{[1 + \Sigma_i 1/e_{r,i}(\lambda)]^2}}, \tag{3.2}$$

with

$$\mathrm{e_{r,i}}(\lambda) = \frac{2(\mathrm{f}(\lambda) + \mathrm{f_{r,i}})}{\mathrm{g_{r,i}}}, \tag{3.3}$$

and

$$i = 0, 1. \tag{3.4}$$

Chapter 4

Transmission features for small and large samples

4.1 Introduction

From Chapter 2 we can get an intuitive understanding of the influence of the array size on the extraordinary transmission. The larger the number of holes in the array, the more light is transmitted with respect to the surface area.

Miyamaru and Hangyo [15] studied the effect of the number of holes on the extraordinary transmission for small numbers of holes. They found there is a linear relation between the height of the peak in the normalized transmittance and the number of holes. This is in accordance with expectations. The amount of transmitted light is proportional to the open area, given by the number of holes n. The signal we measure is proportional to n^2, because $I \propto E^2$. This means the relation between the area and the transmittance is linear.

Here we will study the transmission for different spot sizes, with much larger array sizes than used in Ref[15].

4.2 Extraordinary transmission - first results

In Figure 4.1 we see the transmission as a function of the wavelength (dots). The solid line shows the fit to this data. Rayleigh's anomaly is indicated by the solid vertical line and Wood's anomalies are shown by the dashed and the dashed dotted lines. The first Wood anomaly is caused by SPPs launched on the Air/Gold interface for the (10) direction. The second Wood's anomaly corresponds to the (11) direction at the Au/Glass interface.

Rayleigh's anomaly is calculated from the first Wood anomaly and should

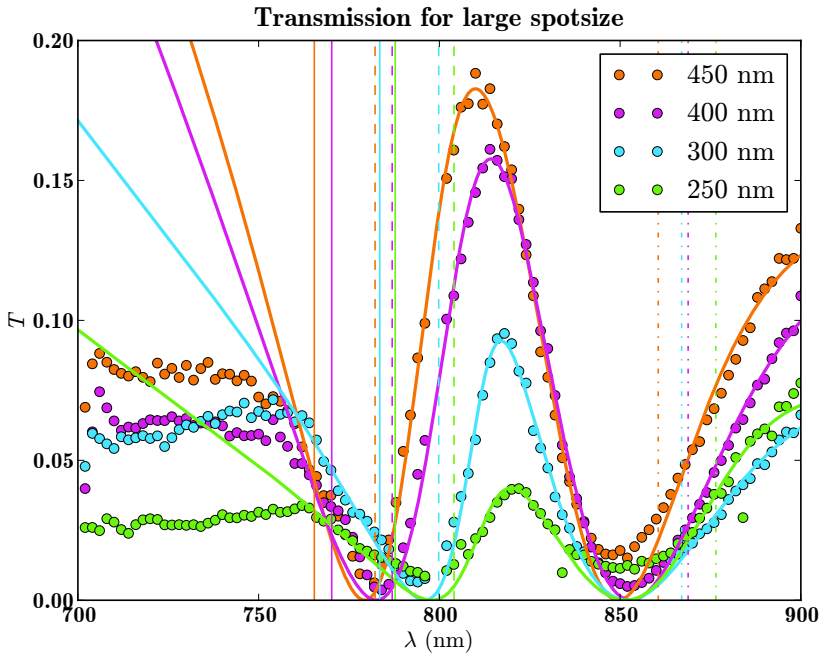

Figure 4.1: This graph shows the transmittance for different hole sizes. The laser power is measured for each wavelength between 700 and 900 nm, with steps of 2nm. The transmitted power was divided by the inserted power, giving us the transmittance. The illumination was done with a large spot size. The wave length for Rayleigh's anomaly by the solid vertical lines. The Wood anomaly is indicated b the dashed line (Air/Au (10)) and the dashed dotted line (Au/Glass (11)).

correspond with the grating period of the array. The grating periods as well as the calculated values of Rayleigh's and Wood's anomaly are given in Table 4.1. Here we see Rayleigh's anomaly does not correspond with the grating periods measured with the scanning electron microscope. An explanation will be given in Section 4.4. Rayleigh's anomaly is visible in the data by the small kink in the downward slope of the Fano-profile. We did not take the data in the wavelength range of 700 to 750 nm into account, which is why the numerical fit does not follow the data below Rayleigh's anomaly.

In the data we see the same asymmetrical shape that is characteristic for the Fano profile. Therefore the maximum of our graph does not coincide with Wood's anomaly. In the tail of the graph we see a second interference maximum coming. This maximum belongs to Wood's anomaly at the Au/Glass interface in the (11) direction.

4.3 Results for different array sizes

We illuminated our sample with a small (278 ± 4.63 μm^2) and large (934 ± 3.88 μm^2) circularly shaped spots. The number of illuminated holes were respectively 469 ± 164 and 1576 ± 251 holes. With this illumination we stayed well within the total area of our sample, 2500 μm^2. In this section we will discuss the difference in the transmission features for these two spot sizes.

holesize	Grating period (nm)	Rayleigh anomaly (nm)	1stWood anomaly (nm)	Width(THz)	2ndWood anomaly (nm)
250	773.2	787.78 ± 2.94	804.05 ± 2.94	16.29 ± 2.81	876.48 ± 3.54
300	765.8	783.51 ± 1.05	799.82 ± 1.05	17.61 ± 1.14	867.02 ± 2.84
400	770.0	770.22 ± 2.50	786.00 ± 2.50	27.59 ± 2.40	868.82 ± 2.93
450	771.1	764.16 ± 2.54	782.22 ± 2.54	24.43 ± 2.40	860.55 ± 2.13

Table 4.1: Values for the different features of the transmission with large spot size for four hole sizes. The actual values of the grating period are given. Rayleigh's anomaly, Wood's anomaly on the Au/Air interface in the (10) direction, and the width of the resulting transmittance maximum and Wood's anomaly on the Au/Glass interface in the (11) direction.

In Figure 4.2 we see the transmission for four different hole sizes. In each Figure the transmission is given for the small illumination spot size (triangles) and the large illumination (dots) as well as a fit to the large spot size. In Table 4.1 the values for Rayleigh's anomaly and two visible Wood's anomalies from the numerical fit are given.

In all Figures we see that the maxima and minima have the same position for small and large spot size. For the 450, 400 and 300 nm hole size, the maxima and minima of the transmission with a large spot size is more articulated. The minima are higher and the maxima are lower. This is only not the case for the 250 nm hole size.

The smearing out of the transmission features, results in less pronounced extremes. For Rayleigh's anomaly a broader shoulder appears in the data instead of a small kink. In the datasets for 400 nm and 250 nm hole size; we see also that the Au/Glass (11) maximum broadens, and that a shoulder at the place of Wood's anomaly is appearing. This broadening of the second maximum also influences the position of the second minimum. For the 400 nm we see that this minimum s shifted to the blue, and the same can be said for the 250 nm hole size.

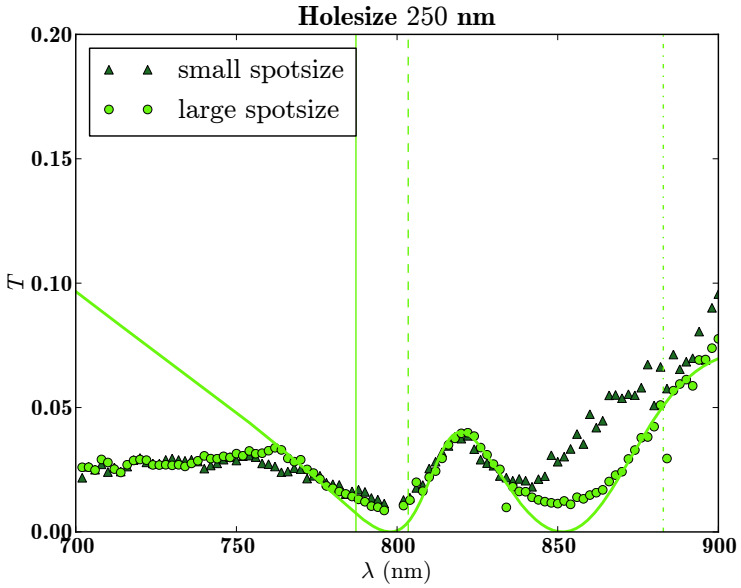

(a) 250 nm

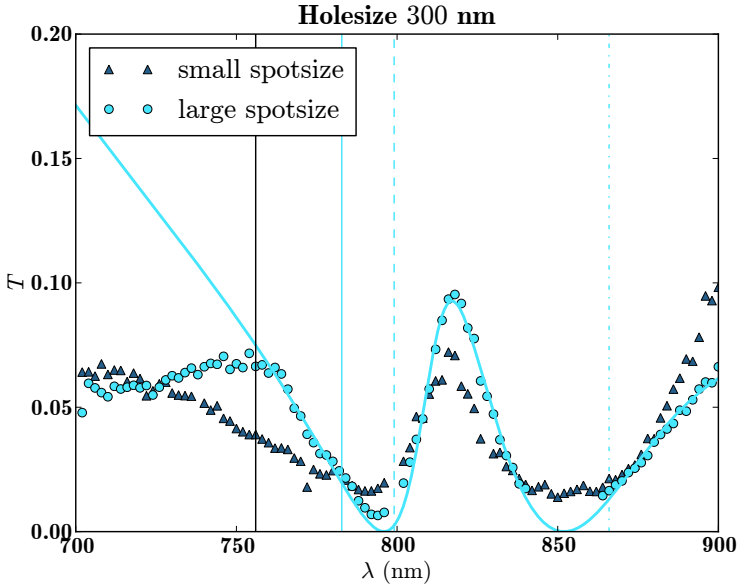

(b) 300 nm

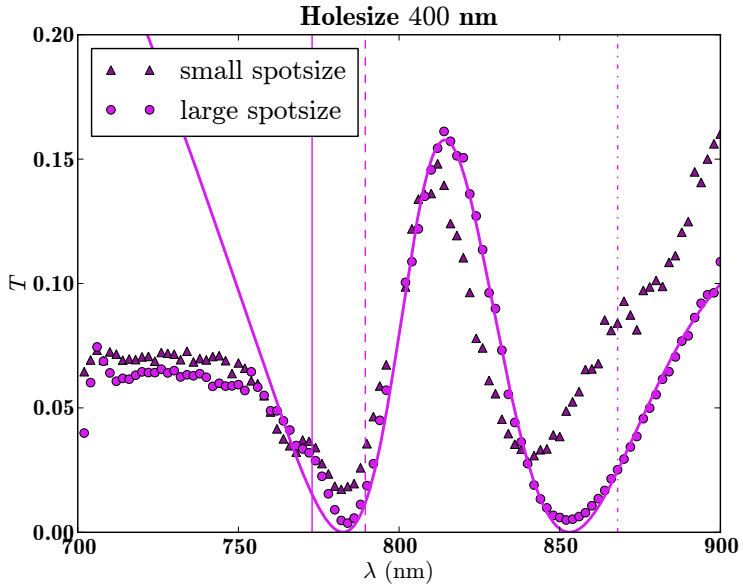

(c) 400 nm

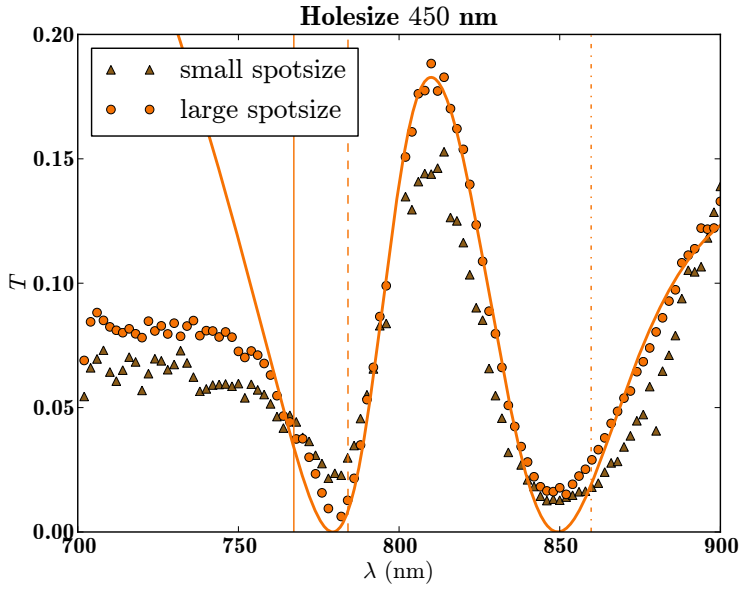

(d) 450 nm

Figure 4.2: Transmission spectrum for two different sample sizes. The sub figures give the transmission for several hole sizes. The solid line indicates Rayleigh's anomaly, Wood's anomaly is indicated by the dashed line (Au/Air (10)) and the dashed dotted line (Au/Glass (11)). The exact values of the anomaly's and the width of Wood's anomaly Au/Air (10) are given in Table 4.1. In Figure 4.2b the data between wavelengths 842 and 862 nm are missing. We did not take these values into account because there appeared to be a temporary offset in the laser power.

4.4 Discussion

Our method of data acquisition and setup prevented us from experimenting with more different array sizes. Still there are some shared features in the results discussed above. In accordance with the data of Miyamaru and Hangyo [15], we find that the transmittance is stronger for larger samples.

We find the same trend as Miyamaru and Hangyo [15], although we cannot confirm the linear relation between the number of holes and the transmittance maximum. Still there are some significant differences between the studies. Miyamaru and Hangyo studied the extraordinary transmission in the far infrared and for very small array sizes (1 to 21 holes). The holes they studied have a circular hole shape and are ordered in a triangular array.

The grating period and the calculated wavelength of Rayleigh's anomaly do not correspond (see also Tabel 4.1). These two values only correspond when the incident light is perpendicular to the interface. Since we could not control the angle of our sample in the setup, and we used unpolarized light, there was an inhomogeneous broadening of the spectrum. Therefore our measurements (and the calculated values from these measurements) for Rayleigh's anomaly are not very accurate.

Chapter 5

Hole size dependence on transmission

5.1 Introduction

The influence of hole properties on the extraordinary transmission have been extensively researched [5, 19, 10, 4]. Prangsma [17] investigated the transition radiation of single rectangular holes as a function of hole width and height. When we look at the results for square holes, we see the radiated power increases with hole size. When we make the distinction between holes in cutoff and not in cutoff, the increase is smaller for the holes that are not in cutoff.

Van der Molen *et. al.* [20] investigated the far field transmittance of a gold array with square holes as a function of hole size. They found that the normalized transmission shows an increasing maximum for increasing hole size. The transmittance does not increase linearly, the slope decreases for larger hole sizes. The results are in accordance with the findings of Prangsma. Additionally, they found a shift in the position of the transmission maxima as a function of hole size. The maxima also broaden for larger holes.

All observed changes in transmittance are gradual. The maxima increase for increasing hole size. Prangsma [17] showed the increase for holes in cutoff is more or less linear. Van der Molen *et. al.* [20] show a gradual increase in transmittance for increasing hole sizes that are not in cutoff. Based on these observations and our assumption that the extra ordinary transmission is a collective effect of the array; we expect the relation between hole size and transmittance to be linear for holes that are in cutoff.

5.2 Normalization

We normalized the transmission to the open area of the 450 nm hole sample. Meaning all results were multiplied by a normalization factor N given by:

$$N = \frac{\text{holesize}^2_{\text{450nm}}/\text{gratingperiod}^2_{\text{450nm}}}{\text{holesize}^2_{\text{sample}}/\text{gratingperiod}^2_{\text{sample}}}. \tag{5.1}$$

The exact normalization factors are given in Table 5.1.

hole size (nm)	normalization factor
250	2.93
300	1.97
400	1.16
450	1

Table 5.1: Normalization factors for the different hole sizes.

5.3 Results

5.3.1 Introduction

In Figure 5.1 we see the transmission normalized to the open area of the 450 nm array. The transmission does not change as a function of hole size for the large holes. The array for 250 nm holes differs from these results. The transmission is lower, and the kink we see in the transmission around 760 nm is stronger for this hole size. The transmission for wavelengths below 760 nm is the same for all hole sizes. This is a background effect that is the same for all arrays.

For the wavelength range we measured, the 250 nm hole array is in cutoff. The 400 and 450 nm hole arrays are not in cutoff. The array that is in cutoff does not support the transverse EM-waves and we measure a smaller transmittance.

The transmission for the 300 nm holes is a special case. For this array the cutoff frequency (indicated by the black line in Figure 4.2b) is close to Rayleigh's anomaly. This influences the transmission spectrum. The most prominent feature is the transmittance in the 700 - 750 nm range. It is significantly higher than the background transmission for the other hole sizes. The shape of the transmission in this range is similar to that of the 250 nm hole array, which is in cutoff. When we look at the maximum (due to Wood's anomaly), the transmission behaves like holes that are not in cutoff.

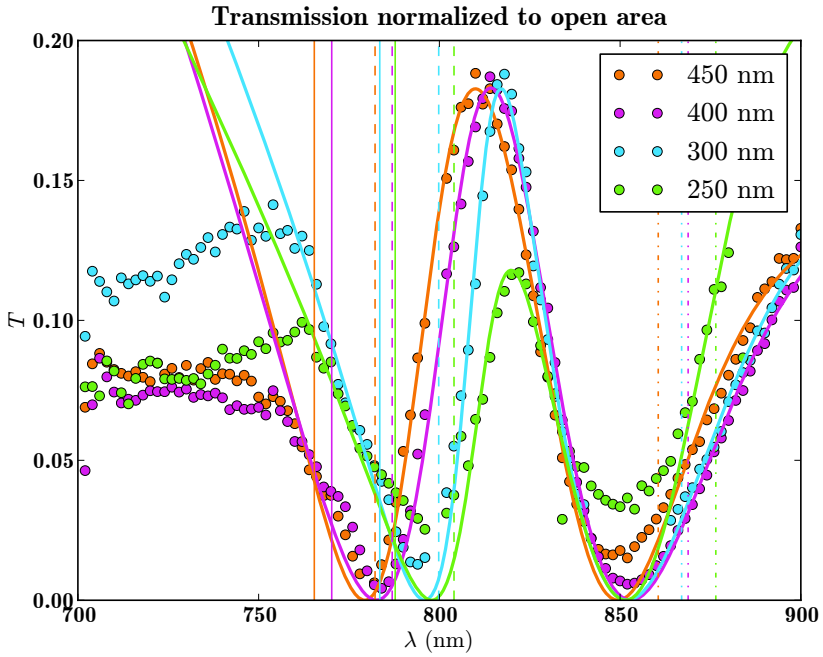

Figure 5.1: This graph shows the transmittance for different hole sizes. The transmittance is normalized to the open area of the 450 nm hole size sample. The normalization factor N for each sample is given in Table 5.1. The laser power is measured for each wavelength between 700 and 900 nm, with steps of 2 nm. The transmitted power was divided by the input power, giving us the transmittance. The illumination was done with a large spot size. The wavelength for Rayleigh's anomaly is indicated by the solid vertical lines. Wood's anomaly is indicated by the dashed line (Air/Au (10)) and the dashed dotted line (Au/Glass (11)).

We describe the ambiguous behavior of the 300 nm hole array to Rayleigh's anomaly and the cutoff frequency being in the same range.

We see that the transmittance peak normalized to open area takes on two values: high for holesizes 400 and 450 nm, and low for hole size 250 nm. The distinction between the arrays with the high and the low transmittance, is that the holes of the array with high transmittance are not in cutoff, whereas the holes of the array with low transmittance are in cutoff. There is no linear relation between holesize and the height of the transmittance peak, instead we see an abrupt change. The transmittance is not dependent on hole size for holes that are not in cutoff. This is not in accordance with what van der Molen *et. al.* [20] showed. For this comparison we left the 300 nm hole size out of the discussion because of the distinctive behavior.

5.3.2 Rayleigh anomaly and Wood's anomalies

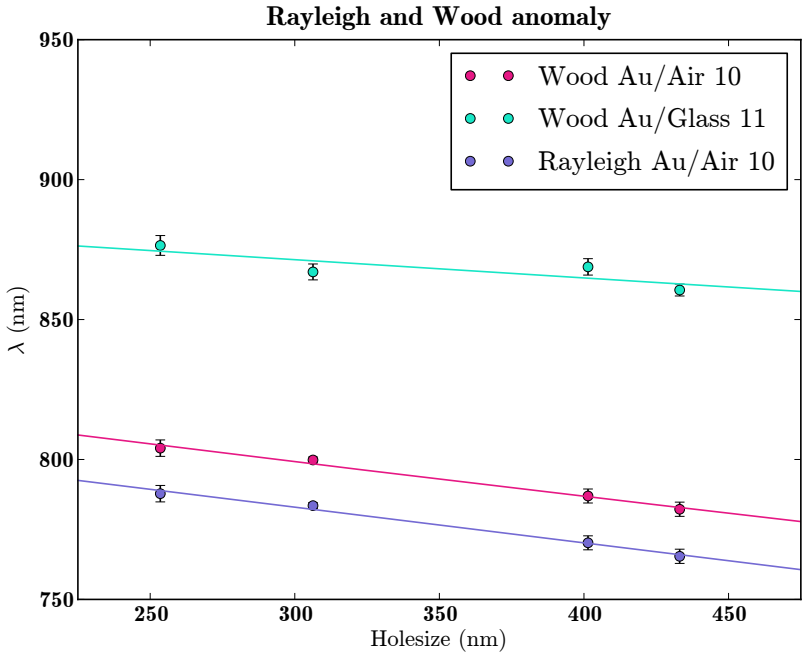

Figure 5.2: This graph shows the values for Rayleigh's and Wood's anomalies for different holesizes and directions in the sample. Values are calculated from the numerical fit to our data.

In Figure 5.2 we see the wavelength of Rayleigh's anomaly and two Wood's anomalies as a function of hole size. Wood's anomalies have a small blue shift when we go to larger hole sizes. Accordingly, Rayleigh's anomaly shows a similar blue shift, because we calculated this value from Wood's anomaly.

The blue shift is not due to the hole size of the different arrays, but to the grating period. Although we aimed for a constant grating period of 763 nm, we showed in Chapter 3 that the grating period is not constant, and increases with increasing hole size. We think the stretching of the array took place in the post baking process.

The large holes have less contact with the glass, and the resist can therefore move more easy, causing a bigger stretch. This might also have happened with the array, leading to a bigger stretch with the big holes. Since there is a linear relation between the hole size and the pitch stretch, we can compensate for this in a next sample.

Besides this drift that can be described to engineering flaws, Wood's anomalies appear to be at a constant position. Exact values of the grating

periods are given in Table 3.1.

5.3.3 Width of interference maximum

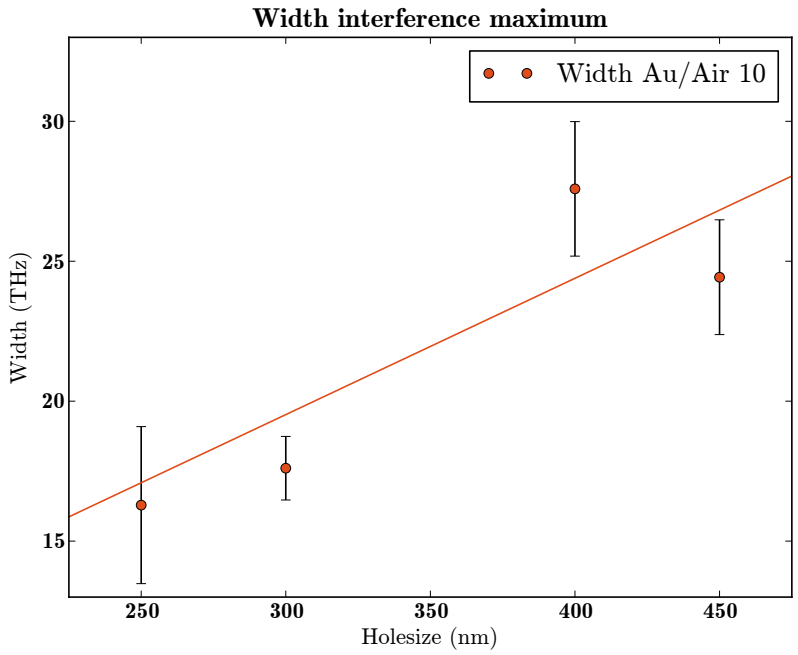

Figure 5.3: This graph shows the with of the transmittance maximum for different hole sizes. The values are calculated from the numerical fit to our data.

Figure 5.3 shows the width of the first interference maximum as a function of hole size. The data support the view that the width increases for increasing hole size. To make any solid statements, further research is required.

5.4 Discussion

5.4.1 Special case: Holesize 300 nm

We did not take the array with hole size 300 nm into account for the comparison of the normalized transmittance. This is because the values we found for the width of the interference and of the second Wood anomaly did not follow the same trend as the other arrays. In the data we could already see that Rayleigh's anomaly does not coincide with the calculated point. Also the shoulder that was present in the transmittance for the other arrays was

not found in these results. The widths of the anomalies for the 300 nm array have in common with the other hole sizes, that the second maximum is broader. But they do not fit in the trend.

There are three possible explanations for this behavior. As we could see, there were several data points left out of the graph, because the laser had an offset there. These data points are at a crucial position for the data fit: exactly at a minimum. Because of the missing data points, the fit could have ended up with wrong values.

A second interpretation is a more physical one. The cutoff wavelength for this hole size is in our measuring domain and is indicated by the black solid line in Figure 4.2b. For the large hole size we see that around this wavelength there is a local maximum.

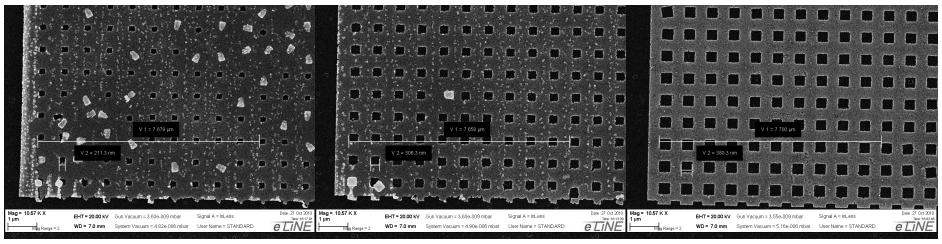

(a) 250 nm **(b)** 300 nm **(c)** 400 nm

Figure 5.4: A rejected array, hole size 200 nm, the 300 nm hole array and the 400 nm hole array. The latter two are both used in this experiment.

Third, it could also be that this array has not the same quality as the other arrays and does therefore not produce data that can be compared. Based on the SEM-pictures of our sample, see Figure 5.4, there is no reason to assume this.

5.4.2 Transmittance

The normalized transmittance we measured did not depend on hole size. This is not in accordance with the observations of Prangsma [17] and van der Molen [20].

Prangsma did transition radiation on rectangular holes. When we look at his results for four square holes, they show an increase in the transmittance for increasing hole size.

Van der Molen *et. al.* studied hole arrays that are in cutoff. For increasing hole size, they see a gradual change in transmission. Since we have only one result for an array in cutoff, we cannot compare our results to the trends

that are described in the literature. These results indicate however that the transmittance has a different behavior for arrays in cutoff and arrays that are not in cutoff.

Van der Molen *et. al.* also observed a redshift in the transmission maxima, that we did not observe. We think this absence is due to the size of the sample. Where van der Molen *et. al.* look at very small samples (100 μm^2), we have sample of approximately 2500 μm^2. We think the resonance is stronger due to the larger sample and that we therefore see no shifting and spreading in the maxima.

For further discussion it must be noted that the observed redshift in the research of van der Molen is in the 11 Au/Glass maximum, whereas we look at the 10 Air/Au maximum. Maybe the maximum we looked at is fixed because it is captured between to minima.

Chapter 6

Bibliography

[1] W.L. Barnes, W.A. Murray, J. Dintiger, E. Devaux, and T.W. Ebbesen. Surface plasmon polaritons and their role in the enhanced transmission of light through periodic arrays of subwavelength holes in a metal film. *Physical Review Letters*, 92(10):107401–1, March 2004.

[2] H.A. Bethe. Theory of diffraction by small holes. *The Physical Review*, 66(7 & 8):163–182, October 1944.

[3] Q. Cao and P. Lalanne. Negative role of surface plasmons in the transition of metallic gratings with very narrow slits. *Physical Review Letters*, 88(5):057403–1, February 2002.

[4] A. Degiron, H.J. Lezec, W.L. Barnes, and T.W. Ebbesen. Effects of hole depth on enhanced light transmission through subwavelength hole arrays. *Applied physics letter*, 81(23):4327–4329, December 2002.

[5] T.W. Ebbesen, H.J. Lezec, H.F. Ghaemi, T. Thio, and P.A. Wolff. Extraordinary optical transmission through sub-wavelength hole arrays. *letters to nature*, 391:667–669, February 1998.

[6] R. Gordon, A.B. Brolo, A. McKinnon, A. Rajora, B. Leathem, and K.L. Kavanagh. Strong polarization in the optical transmission through elliptical nanohole arrays. *Physical Review Letters*, 92(3):037401–1, January 2004.

[7] D.J. Griffiths. *Introduction to Electrodynamics*. Prentice-Hall International, Inc., third edition, 1999.

[8] D.E. Grupp, H.J. Lezec, T.W. Ebbesen, K.M. Pellerin, and T. Thio. Crucial role of metal surface in enhanced transmission through subwave-

length apertures. *Applied physics letter*, 77(11):1569–1571, September 2000.

[9] Y. Zhao I. Acrutsky and V. Kochergin. Surface-plasmon-assisted resonant tunneling of light through a periodically corrugated thin metal film. *Optics Letters*, 25(9):595–596, May 2000.

[10] K.J. Klein Koerkamp, S. Enoch, F.B. Segerink, N.F. van Hulst, and L. Kuipers. Strong influence of hole shape on estraordinary transmission trhough periodic arrays of subwavelength holes. *Physical Review Letters*, 92(18):183901–1, may 2004.

[11] P. Lalanne and J.P. Hugonin. Interaction between optical nano-objects at metallo-dielectric interfaces. *Nature Physics*, 2(x):551–556, x 2006.

[12] P. Lalanne, J.C. Rodier, and J.P. Hugonin. Surface plasmons of metallic surfaces perforated by nanoholes surface.

[13] H.J. Lezec and T. Thio. *Optical Express*, 12(x):3629–51, x 2004.

[14] L. Martín-Moreno, F.J. García-Vidal, H.J. Lezec, K.M. Pellerin, T. Thio, J.B. Pendry, and T.W. Ebbesen. Theory of extraordinary optical transmission through subwavelength hole arrays. *Physical Review Letters*, 86(6):1114–1117, February 2001.

[15] F. Miyamary and M. Hangyo. Finite size effect of transmission property for metal hole arrays in subteraherx region. *Applied Physics Letters*, 84:2742–2744, 2004.

[16] J.A. Porto, F.J. García-Vidal, and J.B. Pendry. Transmission resonances on metallic gratings with very narrow slits. *Physical Review Letters*, 83:2845, april 1999.

[17] Jord Prangsma. *Local and dynamic properties of light interacting with subwavelenth holes*. PhD thesis, Universiteit Twente, Mei 2009.

[18] T. Thio, H.F. Ghaemi, H.J. Lezec, P.A. Wolff, and T.W. Ebbesen. Surface-plasmon-enhanced transmission through hole arrays in cr films. *Optical Society of America*, 16(10):1743–1748, October 1999.

[19] K.L. van der Molen, K.J. Klein Koerkamp, S. Enoch, F.B. Segerink, N.F. van Hulst, and L. Kuipers. Role of shape and localized resonances in extraordinary transmission through periodic arrays of subwavelenght holes: Experiment and theory. *Physical Review B*, 72(4):045421(9), 2005.

[20] K.L. van der Molen, F.B. Segerink, N.F. van Hulst, and L. Kuipers. Influence of hole size on the extraordinary transmission trhough subwavelength hole arrays. *Applied Physics Letters*, 85:4316–4318, 2004.

[21] Ewold Verhagen. *Subwavelength light confinement with surface plasmon polaritons*. PhD thesis, Universiteit Utrecht, December 2009.